International Journal for Multidisciplinary Research (IJFMR)
E-ISSN: 2582-2160 ● Website: www.ijfmr.com ● Email: editor@ijfmr.com

An Effective Strategy for the Photocatalytic Elimination of Industrial Wastewaters *via* MgFe-LDH/TiO_2 Heterojunction

Alaka Samal[1,*], Dipti P. Das[2,*]

[1]Department of Chemistry, Utkal University, Bhubaneswar 751 004, Odisha, India,
[2]Central Characterization Department, CSIR-Institute of Minerals and Materials Technology, Acharya Vihar, Bhubaneswar 751 013, Odisha, India
Email:samal.alaka@gmail.com; diptidas@immt.res.in

Abstract

Reactive dyes are presently the most common type of dye utilised by the garment sector to colour wool, cotton, and viscose-based clothing. By using the typical biological degradation & sediment absorb approaches, it is quite impossible to get rid of them. Thus reactive dye colors in the effluent are major environmental issues in recent times. In this work Reactive dye series has been choosen for the photocatalytic degradation studies over calcined form of TiO_2 and MgFe-LDH_{cal} nanocomposites (TiO_2/MgFe-LDH_{cal}). This work assesses, a detailed investigation of the photocatalytic degradation of the reactive class dyes *Ca*. Reactive green 19, Reactive red 120, Reactive blue 4 and Eosin Yellowish dye by layered double hydroxide (LDH) and TiO_2 heterojunction (MgFe-LDH_{cal}/TiO_2). Here for the first time, photocatalytic application of the said heterojunction was investigated toward the degradation of the reactive dyes. As these dyes are cytotoxic, mutagenic, and inhibit certain mitochondrial functions and often are carcinogens. This heterojunction system degrades the reactive dyes in 1 hour of visible light irradiation. The said LDH heterojunction was characterised by powder XRD to confirm the phase and composite formation, Uv-Visible and PL spectra to know the optical activity of the material in presence of light. The size, interplanar spacing and morphology of the nanoparticles were inspected by HR-TEM analysis. All the batch experiments were carried out at room temperature, without any adjustment of pH, at the dye concentration varying from 20 to 50 mg/L. Furthermore, according to the rejuvenation study, the prepared LDH heterojunction system could potentially be put to use for a number of cycles.

Keywords: MgFe-LDH, TiO_2, reactive dyes, photocatalytic degradation, VAT dyes

1. Introduction

Water is used extensively throughout the dyeing and finishing processes in textile manufacturing. Due to the widespread usage of reactive dyes, wastewaters released into waterways or wastewater treatment plants are heavily polluted. Because of this reactive class dyes utilization in huge quantities, a sizable portion of these dyes enter to the environment through wastewater, hence threatens the environment. Pollution of the environment and lately have increased consciousness about the possibility of worldwide catastrophe. The creation of environmentally friendly, low-energy cleanup technology is a critical undertaking for the sustainable growth of human society. Even extremely small levels of colors in water

from factories could be easily observed through naked eye, and the breakdown byproducts from these reactive dyes can often be hazardous.[1] The textile manufacturing effluents tend to be brightly coloured and dumping into open seas provides an environmental issue since dye concentration typically ranges from 10 to 200 ppm.[2] Approximately $7x10^5$ tonnes of dye are manufactured annually, and in total there are more than 10,000 commonly accessible dyes.[3] With the increased usage of a wide range of reactive dyes, damage by these wastewater is becoming more concerning. The majority of dyes utilised by clothing industries are not biodegradable and are photo-stable.[4] Such effluent must be treated before being released into the environment in order to mitigate the danger of environmental degradation.[5] The most crucial oxidation process uses heterogeneous photocatalysts, a mix of TiO_2 and light, to destroy water soluble organic contaminants in water and wastewater. Many methodologies, such as chemical or physical procedures, have been suggested or are being explored in this regard.[6] Due to its resistance to corrosion in water and UV light reacivity, TiO_2 is a frequently used photo-catalyst. TiO_2 has the ability to act as an oxidative and a reductive catalyst. Due to its powerful oxidising properties, non-toxicity, and long-term photostability, TiO_2 is regarded as being very near to the perfect semiconductor for photocatalysis.[7] Although there are some lacuna with TiO_2 photocatalysis, such as lower catalytic active sites, lack of convenient structural properties, and a wide band gap energy (3.2 eV), these issues could be resolved by using conventional synthesis methods with other semiconductor photocatalyst combination. Due to their special characteristics, such as tiny particle sizes, high surface to volume ratios, and easy synthesis process, with which they could be fixed onto solid matrices for improved wastewater treatment, nanoscale particles seem promising in this field.[8] Commercial dye degradation by TiO_2-mediated photocatalytic oxidation looks to be a promising method. Organic contaminants found in waste streams can be effectively mineralized into CO_2 and inorganic ions by heterogeneous advanced oxidation processes that utilise hydroxyl radicals (•OH).[9,10]. TiO_2 has a significant potential for industrial applications in the photocatalytic remediation of water contaminants due to its low cost and ease of manufacture. A cost-effective technique is required to remove colours from municipal and industrial water effluents due to increased environmental concerns and awareness. A potential technique to induce degradation of dyes includes the oxidation process through TiO_2. By using heterogeneous advanced oxidation techniques that make use of hydroxyl radicals (•OH), organic pollutants present in waste streams may be effectively broken down into CO_2 and other inorganic ions. [9,10] Due to its low cost and simplicity in manufacturing, TiO_2 has enormous possibilities for usage including photocatalytic treatment of water-based pollutants. Owing to the increasing environmental consciousness and concerns, a low-cost approach is needed for eliminating hazardous water contaminants from urban and industrial wastewater discharges. Water soluble, brightly colored dyes provide the greatest removal challenges, including reactive and acid dyes. Both types of dyes have been shown to be ineffective when treated by traditional and urban oxygenation treatment methods.[11,12] Currently, there is a lot of interest in the growth of visible light reactive catalysts for the efficient and sustainable harvesting of the 43% visible light present in solar radiation. Numerous studies have been conducted on titanium dioxide (TiO_2) as a photocatalyst for the conversion of solar energy and the degradation of pollutants. [13,14] The introduction of advanced oxidation processes for the treatment of waste fluids is the subject of several studies. [15,16] Recent studies have documented the breakdown of organic dyes brought on by the use of Layered Doubled Hydroxides (LDH) based photocatalysis.[17-20] For the development of LDH materials with effective photocatalytic capabilities, many approaches have been taken. LDH hybrids were recently created using carbon-based components and semiconductors to improve photocatalytic activity. [17]

Alternately, incorporating cations in the layers that showed enhance photocatalytic activity due to the flexible composition of LDHs were shown by many researchers. In fact, binary and ternary LDHs and materials generated from LDH have demonstrated promising photocatalytic properties when replaced with transition metals were well documented by the researchers recently. [18] For instance, the n-type semiconductor NiFe LDH [19] that absorbs visible light up to 800 nm and have extraordinary photoactivity as compared to other LDH materials was reported. Recently published article [20] also depicts the visible light activity in the remediation of water pollutants by ternary ZnCoFe LDH. But no investigation has been done by using Mg-Fe-LDH based TiO_2 composites till date despite of its narrow band gap, high visible light absorptive capability, stability and economic features.

Apart from doping and composite synthesis by using carbon based materials, LDH material, which consists of special 2D morphology along with typically positively charged brucite-like host layers, inspires us for the preparation of heterojunction hybrid with TiO_2 photocatalyst. In this article, first ever attempt has been made to synthesize visible light active heterojunction MgFe-LDH_{cal}/TiO_2 for photocatalytic degradation of VAT class dyes present in waste waters collected directly from local textile industries (Sambalpuri Vastralaya, Odisha, India) as well as laboratory prepared sample waste water (for reactive class dyes degradation) in very high concentration.

2. Experimental

2.1. Apparatus and reagents

XRD, diffuse reflectance UV (DRUV)-Vis, photoluminescence, TEM, and energy dispersive X-ray (EDX) investigations and analysis were used to characterize all of the as prepared composites. CuKα radiation with 2θ ranging from 10º to 80º at a scanning rate of 5º per minute was used in a Rigaku Miniflex powder diffractometer (operated at 30 kV and 15 mA) to acquire Xray diffraction patterns. With Barium Sulfate used as a reference, the DRUV-Vis spectra of the catalyst samples were collected using a Varian Cary 100 spectrophotometer outfitted with a diffuse reflectance accessory in the wavelength range of 200–800 nm. PL spectra were captured using a Perkin-Elmer LS 55 fluorescence spectrometer with 380 nm excitation at room temperature. An FEI TECNAI G2 model running at 200 kV was used to capture the TEM pictures. the study's sampling. For preparing materials for the experiment, the as-prepared catalytic composites were sonicated in 2-propanol for 3 min. The samples were then drop-dried on a copper grid coated with carbon film.

Titanium isopropoxide (purity >97%, Sigma Aldrich), Isopropanol (purity >99%, Sigma Aldrich), $Mg(NO_3)_2.6H_2O$ and $Fe(NO_3)_3.9H_2O$ (Alfa Aesar). No additional purification was performed on any of the compounds utilised.

2.2. Synthesis of catalysts

2.2.1. Synthesis of TiO_2

Initially, anatase TiO_2 was synthesized by the following method. 10 ml titanium isopropaxide was mixed with 60 ml of Isopropanol. Then deionised water in the amount of 3 ml was then added to the solution. The mixture was vigorously stirred until a cloudy solution was obtained. Then the solution was centrifuged by laboratory centrifuge equipment at 5000 rpm for 30 min. Then the precipitate was dried at 80 ºC for overnight. The dried precipitate grinded with a mortar until fine white powder was obtained. The powder was then calcined in a muffle furnace at 500 ºC.

2.2.2. Synthesis of MgFe-LDHcal

Then MgFe-LDH was synthesized by taking an aqueous solution of $Mg(NO_3)_2.6H_2O$ (0.22 mol) and $Fe(NO_3)_3.9H_2O$ (0.11 mol) in 200 ml of distilled water. The NaOH (0.72 mol) solution was added drop wise in the above mixture and then undergone with vigorous stirring at room temperature for 2 h. Then, the mixture was aged at 60 °C for 18 h. The precipitate formed was filtered and washed with hot distilled water until there is a neutral pH of the filtrate was obtained. Finally, the powder was dried in an oven at 80 °C overnight. Then, it is calcined at 800 °C for 4 h. After the cacination process at high temperature, the LDH is now named as MgFe-LDHcal.

2.2.3. Synthesis of MgFe-LDHcal/TiO2 heterojunction

To form the heterojunction, different wt.% of calcined MgFe-LDH powders (2, 5, and 10) were loaded onto TiO_2 by the in-situ growth of TiO_2 nanoparticles on its layers. Then, it is calcined at 500 °C for 4 h and these were designated as xMgFe-LDHcal/TiO_2 heterojunction. These products were applied for the photocatalytic degradation experiments.

2.3. Photocatalytic Experiment

A stoppered Pyrex conical flask that contained the catalyst (20 mg) and 20-50 mg/L of dye concentration was exposed to visible light in an illumination UV-Vis. chamber (BS 02, Germany) for 1 h. The photodegradation of laboratory prepared organic textile dyes namely Reactive green 19, Reactive red 120, Eosin Yellowish and Reactive blue 4 were observed. Additionaly, direct industrial waste water treatment was carried out with dye concentrations (209 mg/L for BLUE VAT DYE and 1657 mg/L for VIOLET VAT DYE collected from local textile industry) with 1 h of visible light irradiation. All the experiments were performed at room temperature without adjusting pH of the experiments. After reaction completion, the results were analysed in Uv-Visible spectrophotometer.

2.4. Photocatalytic Experiment

A stoppered Pyrex conical flask that contained the catalyst (20 mg) and 20-50 mg/L of dye concentration was exposed to visible light in an illumination UV-Vis. chamber (BS 02, Germany) for 1 h. The photodegradation of laboratory prepared organic textile dyes namely Reactive green 19, Reactive red 120, Eosin Yellowish and Reactive blue 4 were observed.

Scheme 1. Photoreactor with highly concentrated indstiral waste collectced from sambalpuri bastryalaya industry.

The direct industrial waste water treatment was carried out with dye concentrations (209 mg/L for BLUE VAT DYE and 1657 mg/L for VIOLET VAT DYE) with 1 h of visible light irradiation through a Lelesil photoreactor with MPMVL Lamp. All the experiments were performed at room temperature

without adjusting pH of the experiments. After reaction completion, the results were analysed in Uv-Visible spectrophotometer.

3. Results And Discussion

3.1. XRD patterns of the samples

Representative XRD patterns of the samples exhibit the characteristic reflections of the LDH materials. [21,22] XRD spectra (Figure 1) show significant formation of semiconductor TiO_2 and MgFe-LDH in the synthesis method. The TiO_2 nanoparticles exhibited pure anatase phase in case of pristine as well as in the synthesized composite. This reflects the transition of the TiO_2 nanoparticles structure at a calcination temperature of 500 ^oC. The high intensity located 2θ = 35.54, 43.21, 62.75 represents the peak 511, 400, 440 show the formation of heterojunction. The XRD patterns of the as-synthesized xMgFe-LDH/TiO_2 solids indicate the formation of a well crystallized layered structure. The calculated basal spacing values corresponding to the (220) and (511) planes indicates at 2θ= 30^o, 57^o were easily recognized in all the patterns for MgFe-LDH in the calcined form. The XRD pattern indicates planes (101), (004), (200) refer to 2θ= 25^o, 37^o and 37^o point out the TiO_2 is in anatase phase. Thus heterojunction formation was confirmed from the XRD pattern with having both the diffraction pattern.

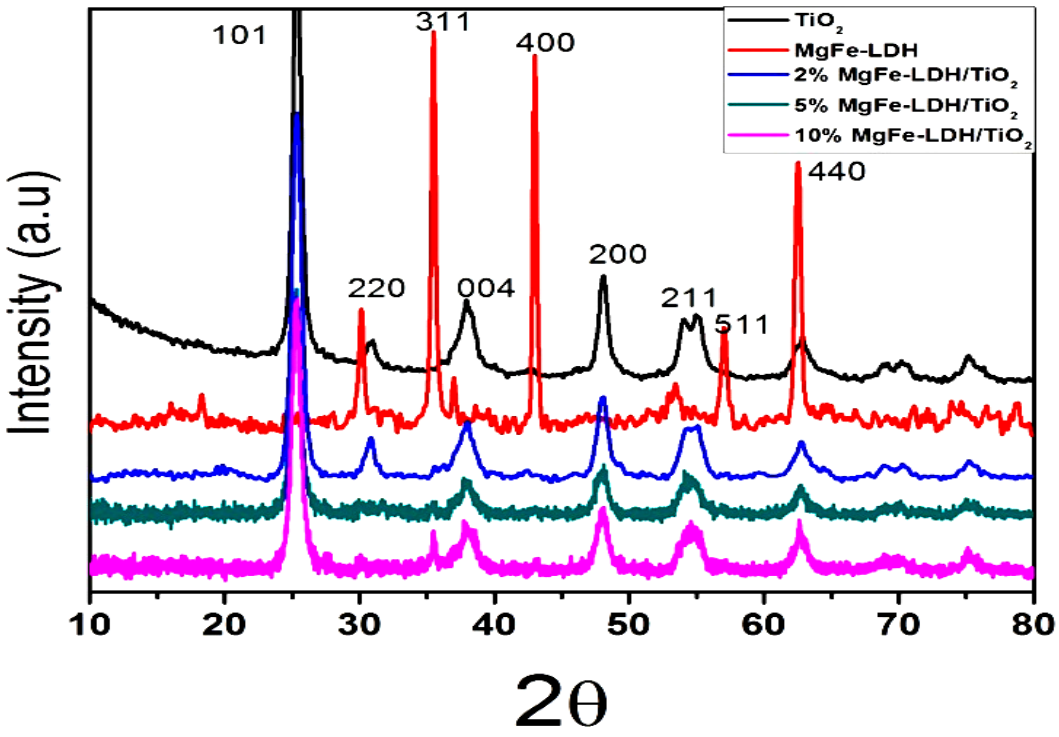

Figure 1. XRD patterns of xMgFe-LDH/TiO_2 heterojunction.

3.2. Uv-Vis DRS Analysis

The optical absorption behaviour of the TiO_2, MgFe-LDH_{cal} and its heterojunction was conducted by UV-vis absorption spectroscopy and is depicted in Figure 2, the absorption edge shifted towards longer wavelength, indicated enhanced photocatalytic activity of the heterojunction upon illumination of visible light. UV/Vis diffuse reflectance spectra of xMgFe-LDH_{cal}/TiO_2 heterojunction absorbs the broad range of radiation unlike pure TiO_2. This consequently shows that these heterojunction should have good photo activity in presence of visible spectrum of solar radiation.

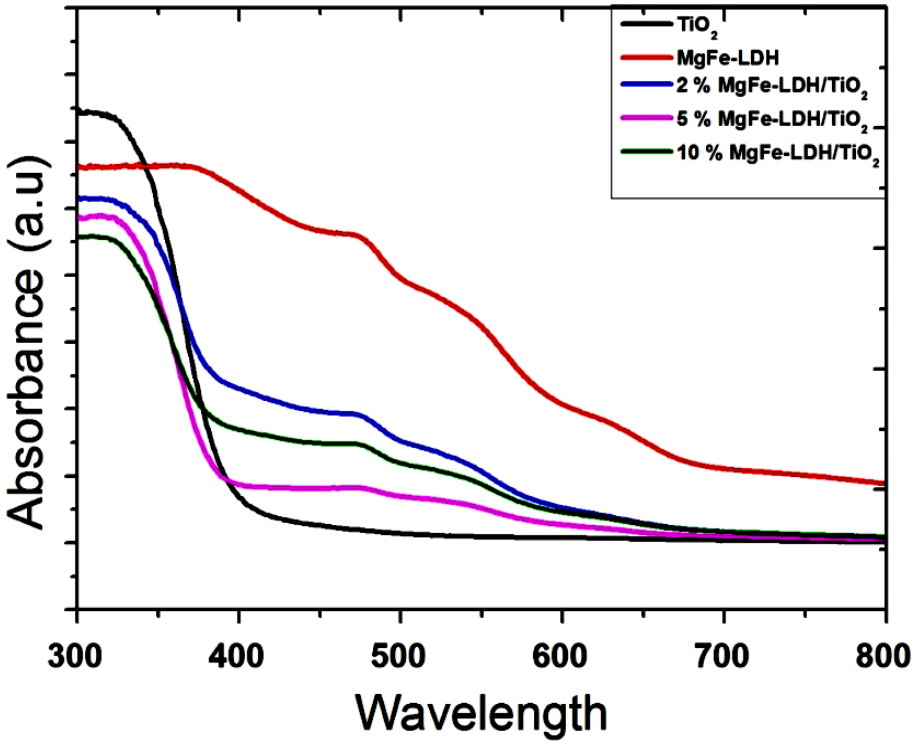

Figure 2. UV-Vis DRS spectra of TiO_2, MgFe-LDH_{cal} and xMgFe-LDH_{cal}/TiO_2 heterojunction (x=2, 5, 10 wt. %).

3.3. Photoluminescence Study

PL spectroscopy of TiO_2, MgFe-LDH_{cal} and MgFe-LDH_{cal}/TiO_2 shows emission peaks at 540 nm upon excitation at 350 nm. In the above spectra pure TiO_2 shows the highest charge carrier recombination thus having the highest intensity. Pure MgFe-LDH_{cal} also shows high intensity, with elevated charge carrier recombination property. But at the same time as the heterojunction designed with the weight percentage of 5MgFe-LDH_{cal}/TiO_2 has the lowest intensity as compared to the other synthesized composites and so it is showing best activity towards photocatalytic reaction. The spectrum region or comparative intensity of peaks are unaffected by the formation of heterojunction, but the overall emission intensity is gradually decreased. Our model predicts the decrease in PL intensity following semiconductor insertion with the LDH heterojunction formation, charge separation occurs which diminishes the recombination of photogenerated charge carriers and hence the lowest intensity.

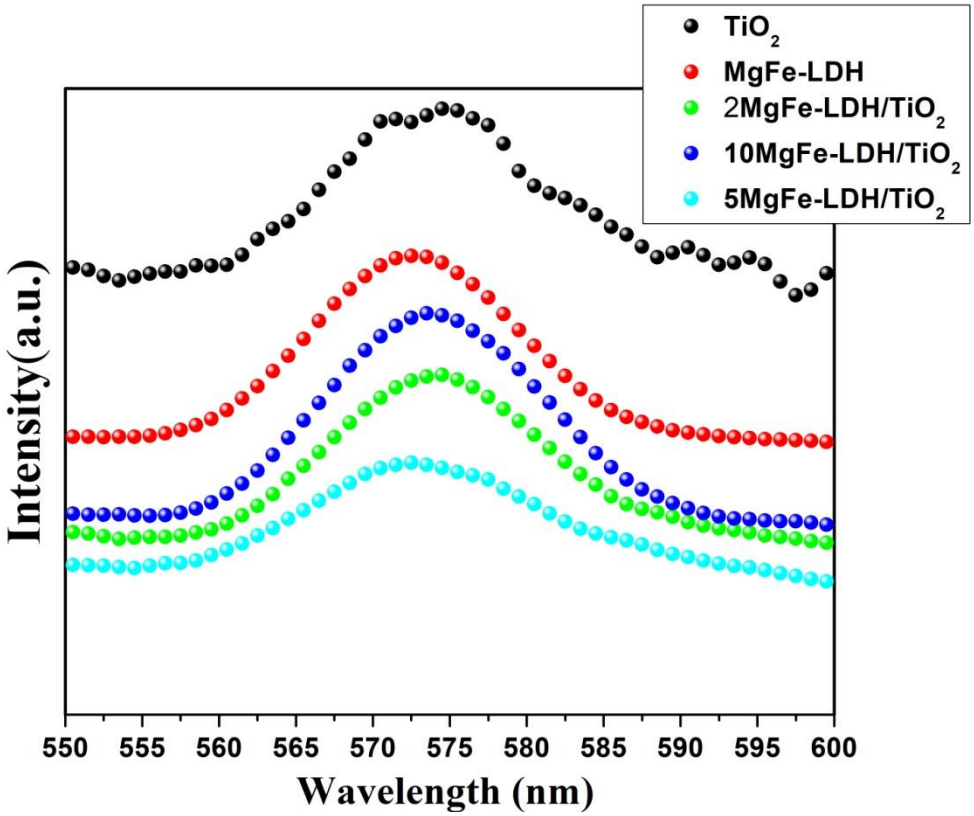

Figure 3. PL spectra of TiO_2, MgFe-LDH_{cal} and xMgFe-LDH_{cal}/TiO_2 composite (x=2, 5, 10 wt. %).

3.4. Transmission electron microscopy Study

From the Morphological study of pure MgFe-LDH_{cal} (Figure 4A), an equi-axed layered morphology with layers having thickness range of 1-2 nm can be observed. Energy dispersive X-ray (EDX) spectroscopy investigation further supports the material's composition with strong Mg, Fe, and O signals may be seen in EDX point spectra that were collected at the layer scan's central spot (Figure 4B). This result implies the absence of impurities during the synthesis of photocatalysts. The elemental mapping images (figure 4C-G) clearly indicate that the MgFe-LDH_{cal} nanolayers consist of Mg, Fe, and O atoms. Interestingly, thin layers consist of O-Mg-Fe trimetal and are covered homogeneously with other atoms. From the Morphological study of pure MgFe-LDH_{cal} (Figure 4A), an equi-axed layered morphology with layers having thickness range of 1-2 nm can be observed. With the use of energy dispersive X-ray (EDX) spectroscopy investigation, the elemental content is further verified.

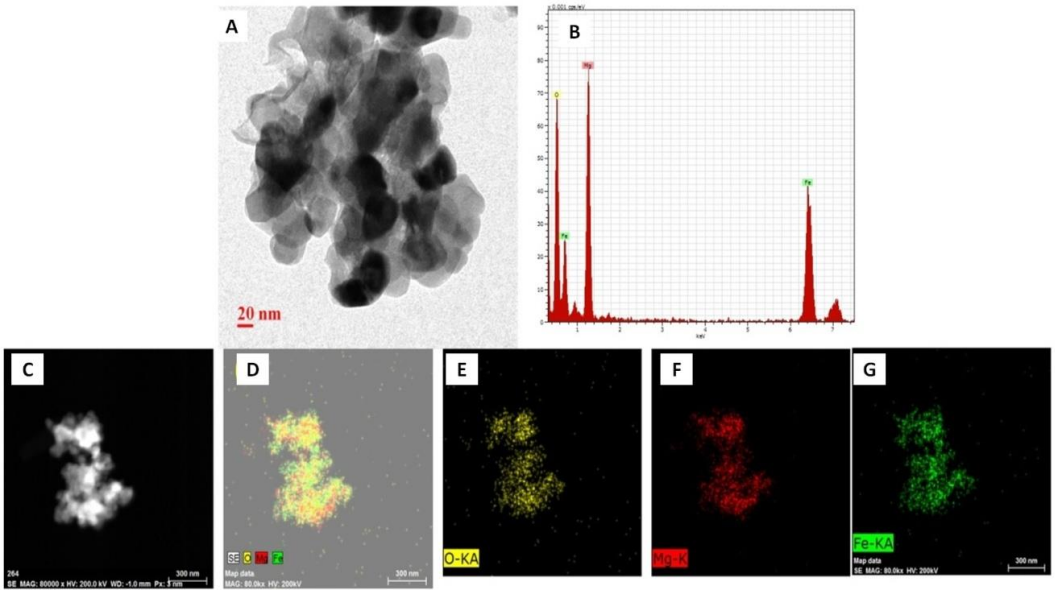

Figure 4. Shows the (A) TEM image of MgFe-LDH pure after calcination. (B) EDX spectra of MgFe-LDH showing the presence of Mg,Fe and O elements in the photocatalyst. (C-G) Elemental mapping analysis in the same area of the MgFe-LDH, showing the presence of O, Mg, Fe elements without any other impurities.

To gain a better insight into the chemical nature of the deposits, TEM-guided Energy-dispersive X-ray spectroscopy (EDX) analysis was performed on selected sample 5MgFe-LDH_{cal}/TiO_2 after calcinations (Figure 5) and EDX chemical analysis made it possible to determine their elemental composition. The TEM image of 5MgFe-LDH_{cal}/TiO_2 heterojunction shows beautiful nanoparticles with pseudo spherical shapes and average diameter of 7-12 nm (Figure 5A) on the thin layers of MgFe-LDH_{cal}. This again evidenced the formation of heterojunstion as the nanopartcles are evenly distributed on the surface of layered structure. The structures have a strong elemental signal (Figure 5C-H) of Mg, Fe, O and Ti which confirms the successful synthesis of the heterojunction without any impurity.

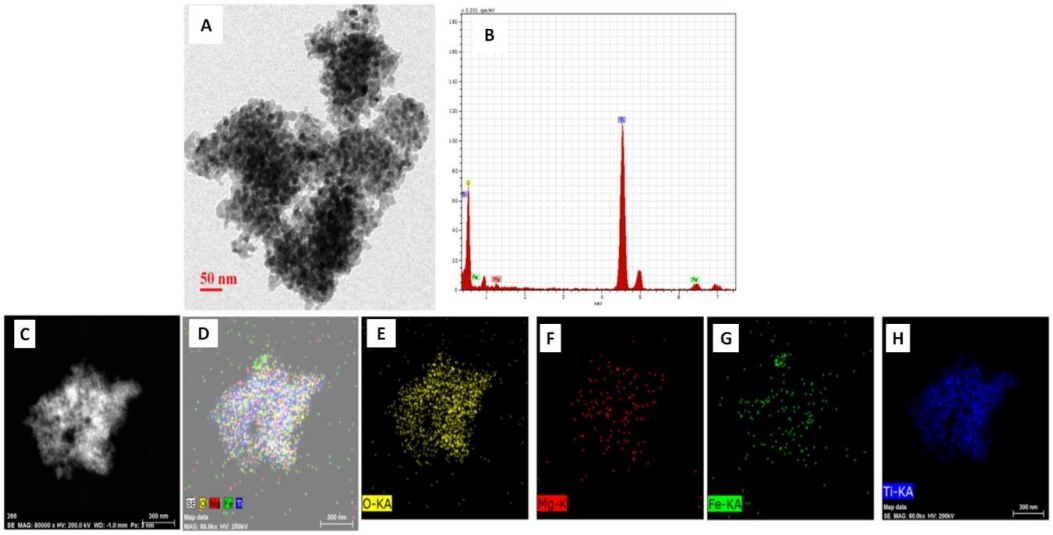

Figure 5. Shows the (A) TEM image of 5MgFe-LDH_{cal}/TiO_2 after calcination. (B) EDX spectra of 5MgFe-LDH_{cal}/TiO_2 showing the presence of Mg, Fe, Ti, and O elements in the photocatalyst. (C-

H) Elemental analysis of the 5MgFe-LDH$_{cal}$/TiO$_2$, showing the presence of O, Mg, Fe, Ti elements without any other impurities.

To gain a better insight into the chemical nature of the deposits, TEM-guided Energy-dispersive X-ray spectroscopy (EDX) analysis was performed on selected sample 5MgFe-LDH$_{cal}$/TiO$_2$ after calcinations (Figure 5) and EDX chemical analysis made it possible to determine their elemental composition. The TEM image of 5MgFe-LDH$_{cal}$/TiO$_2$ heterojunction shows beautiful nanoparticles with pseudo spherical shapes and average diameter of 7-12 nm (Figure 5A) on the thin layers of MgFe-LDH. This again evidenced the formation of heterojunstion as the nanopartcles are evenly distributed on the surface of layered structure. The structures have a strong elemental signal (Figure 5C-H) of Mg, Fe, O and Ti which confirms the successful synthesis of the heterojunction without any impurity. The lattice images of LDH layers and nanoparticles were clearly observed, which indicated that these have high degrees of crystallinity and phase purity. From the distance between the adjacent lattice fringes, we can assign the lattice plane on the LDH layer and TiO$_2$ nanoparticles. The pure MgFe-LDH$_{cal}$ layer shows the interplaner spacing of d = 0.45 nm for the (311) plane, which is consistent with the XRD value (figure 6a). Interestingly, in the HRTEM images of the heterojunction of 5MgFe-LDH$_{cal}$/TiO$_2$ the TiO$_2$ nanoparticles showed very clear lattice spacing of d = 0.33 nm for the (101) plane of the anatase phase on the layer of MgFe-LDH$_{cal}$ layer having the lattice fringes with interplanar spacing of d = 0.45 nm as shown in figure 6B. The distance between the lattice fringes (d = 0.33 nm) in the pseudo sphere can be assigned to the interplanar distance of anatase phase (101) plane, which is well consistent with XRD results as well. Further observation by SAED (inset image in Fig. 6A-B) confirmed that the TiO$_2$ had a polycrystalline anatase structure, and the layer of MgFe-LDH$_{cal}$ were single crystalline when heterojunction with TiO$_2$ was not made. Further HRTEM, TEM and SAED analysis, it can be concluded that the formation of heterojunction affect not only the crystalline phase and crystallinity but also the morphologies of TiO$_2$ nanostructures.

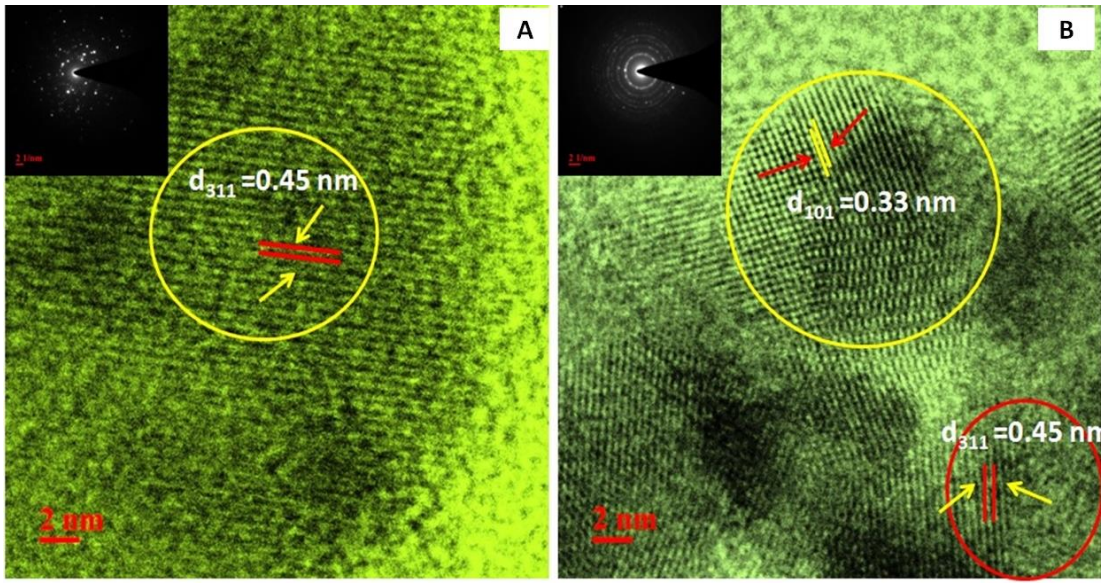

Figure 6. HRTEM images of (A) MgFe-LDH$_{cal}$, (B) 5MgFe-LDH$_{cal}$/TiO$_2$ showing the lattice fringes of the individual planes (inset showing the SAED pattern respectively).

Band gap is the predominant characteristics of any photocatalytic semiconductor which determines the light harvesting efficacy of it. Using the reflectance data, the Kubelka-Munk technique was used to measure the band gap (Eg), which is crucial to test the light-harvesting effectiveness, for the 5MgFe-LDHcal and 5MgFe-LDHcal/TiO_2 samples (Figure 7A and B).[23] Extrapolating the linear component of the $(Ahv)^{1/2}$ curve vs photon energy hυ yielded the value of Eg. A Tauc plot was used to assess the band gap's nature (direct or indirect). Equation (1) provides the Tauc relationship as given below:

$$\alpha h\gamma = A(h\gamma - E_{BG})^n \quad [1]$$

in which a is the absorption coefficient, hν is the energy of the incident radiation, A is the constant based on effective masses of electrons and holes, and n can take the values of 1/2 and 2 for a direct or indirect band gap transition, respectively. In accordance to the equation [1], the band gap of pristine MgFe-LDH_{cal} and 5MgFe-LDH_{cal}/TiO_2 heterojunction were calculated where pristine MgFe-LDH_{cal} shows the indirect band gap transition values of the order of 1.81 eV, which could be suitable for visible-light sensitivity. The 5MgFe-LDH_{cal}/TiO_2 heterojunction displayed two Eg values of 1.8 and 3.1 eV, which are as predicted and is may be correspond to 5MgFe-LDH_{cal} and 5MgFe-LDH_{cal}/TiO_2, respectively.

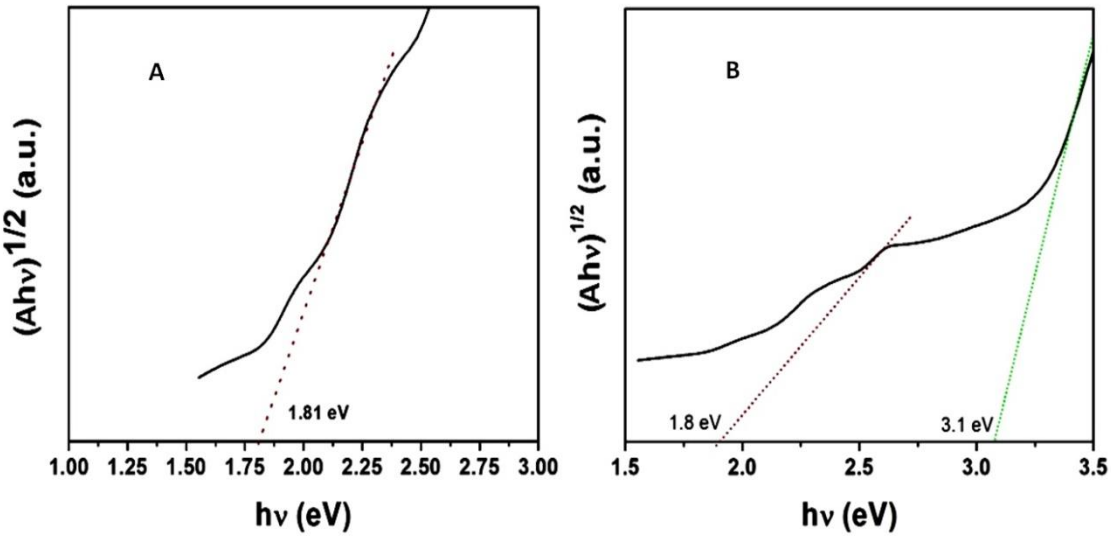

Figure 7. Band gap determination by tauc plot of (A) 5MgFe-LDH_{cal} (B) 5MgFe-LDH_{cal}/TiO_2 heterojunction.

4. Photocatalytic application of the MgFe-LDH_{cal}/TiO_2 heterojunction

As described earlier in the photocatalytic experiment section, the photodegradation of laboratory prepared organic textile dyes namely Reactive green 19 (RG 19), Reactive red 120 (RR 120), Eosin Yellowish (EY) and Reactive blue 4 (RB 4), Rhodamine B (RhB), Rhodamine 6G (Rh 6G), Methylene Blue (MB), Alizarin Red S (ARS) and the direct industrial waste water treatment was carried out with dye concentrations (209 mg/L for BLUE VAT DYE and 1657 mg/L for VIOLET VAT DYE) with 1/1.5 h of visible light irradiation over 5MgFe-LDH_{cal}/TiO_2 heterojunction (figure 8A-C). From the image the high degradation efficacy of the heterojunction can be observed. As all the organic/reactive dyes are getting degraded upto more than 90 % under visible light irradiation. The Figure 8c, showing the high activity of the heterojunction towards the degradation of highly concentrated industrial effluents in the concentration of 209 mg/L for BLUE VAT dye and 1657 mg/L for VIOLET VAT dye. Where after the

dye degradation experiment complete degradation of VIOLET VAT dye was achieved along with 63.8 % degradation of BLUE VAT dye.

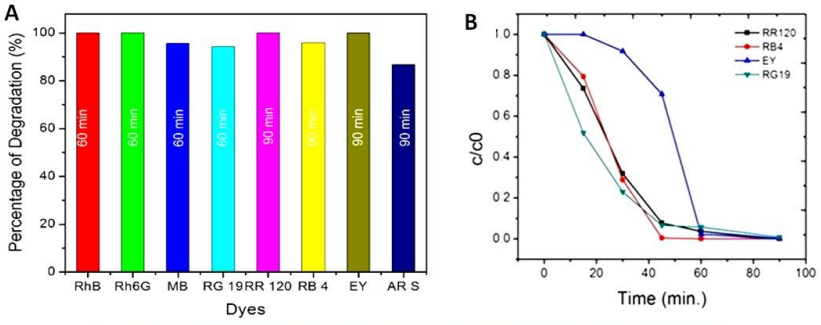

C

Name of Industrial dye	Percentage Of Degradation	Time Of Visible Light Irradiation	Dye Concentration
VIOLET VAT DYE	63.8	1 h	209 mg/L
BLUE VAT DYE	100	1 h	1657 mg/L

Figure 8. (A-B) Degradation efficiency of 5MgFe-LDH$_{cal}$/TiO$_2$ for reactive dyes, (B) Rate of change of concentration of RR120, RB4, EY, RG19 with varying initial concentration over 5MgFe-LDH$_{cal}$/TiO$_2$ at different times. (C) Tabular image showing the degradation of highly concentrated industrial dye effluents collected directly from textile industry.

The photodegradation of any organic/reactive is initiated by de-ethylation and ring-opening pathways. With the purpose to distinguish between these pathways, UV–vis spectra of EY, RB4, RG19, RR 120 were experimented during the degradation reaction over 5MgFe-LDH$_{cal}$/TiO$_2$ sample were showed in figure 9A-D. It is pretty obvious that the degradation response of the dyes over these materials occurs via ring-opening mechanism based on the dwindling in intensity of the primary absorption peaks of all dyes as the irradiation period increases with no variations in peak positions. Additionally, nearly every colours tend to disintegrate within 90 minutes.

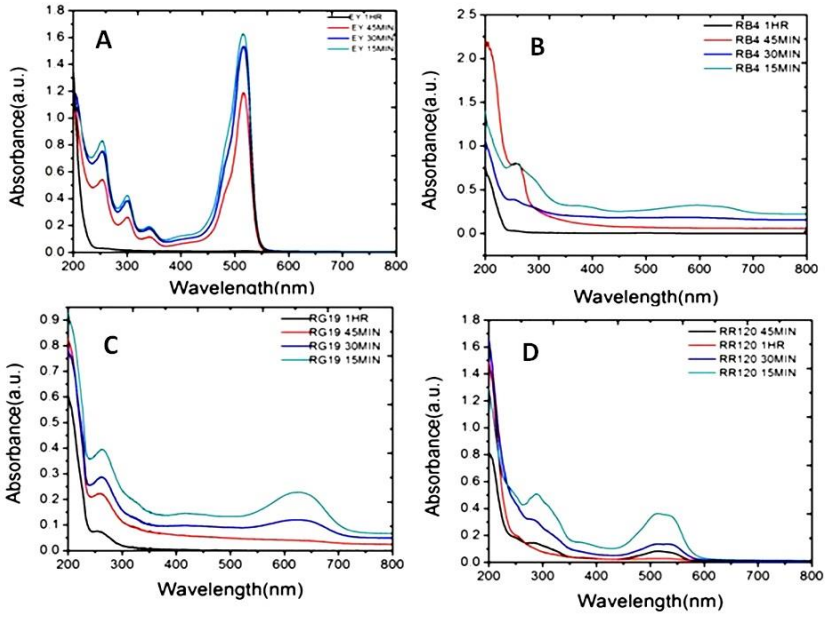

Figure 9. UV–vis spectra for degradation of dyes (A) EY, (B) RB 4, (C) RG 19, (D) RR 120 over 5MgFe-LDH$_{cal}$/TiO$_2$ under visible-light irradiation.

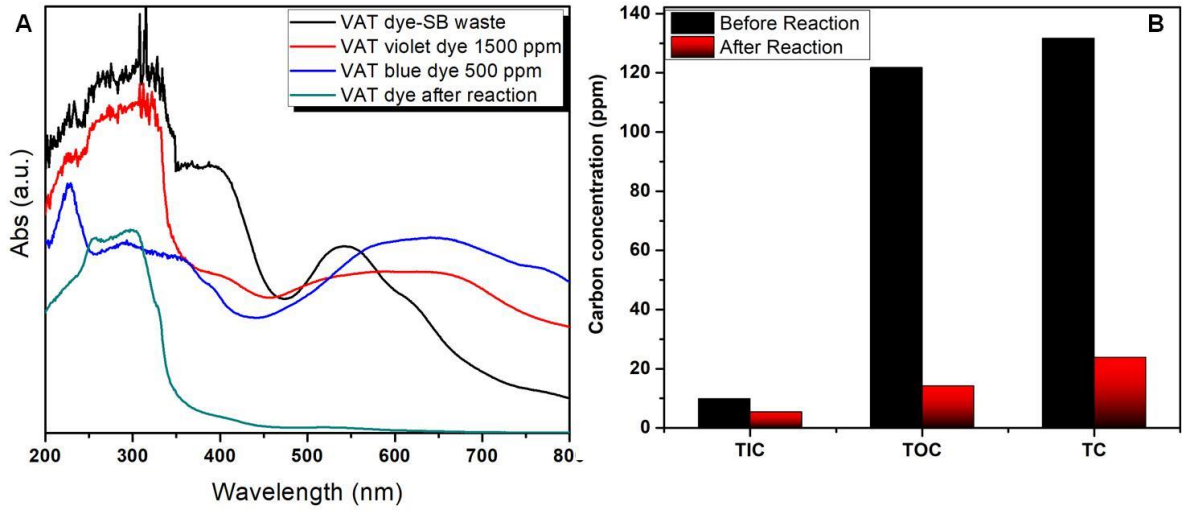

Figure 10. (A) UV–vis spectra for degradation of VAT dyes (B) Total Carbon test over 5MgFe-LDH$_{cal}$/TiO$_2$ under visible-light irradiation.

Again, the efficacy of the heterojunction catalyst was tested by the absorbance spectrum of the VAT dyes collected from the industry as shown in figure 10a. It could be clearly observed from the figure that the industrial effluent has efficiently degraded over the catalyst within 1 h of visible light illumination. From this observation we can conclude that this catalyst is very effective in degrading industrial effluents with very high concentrations. Furthermore, the total carbon (TC) analyses in figure 10b also corroborate the removal of carbon contents after the reaction under visible light in presence of the catalyst from the industrial effluent.

5. Mechanism

Apart from the band gap calculation of both the semiconductors, the conduction band edge potential (CB) and the valence band edge potential (VB) were also calculated of the calcined MgFe-LDH$_{cal}$ to propose a plausible mechanism to explain the enhanced photocatalytic activity of the 5MgFe-LDH$_{cal}$/TiO$_2$ heterojunction as illustrated in figure 11. With the intention of clarifying the separation of photogenerated electron-hole pairs over the said heterojunction, it is necessary to find out the CB and VB potentials of the components. These energy levels were calculated using the following empirical equations [2]:

$$E_{CB} = -\left[\chi A^a \chi B^b \chi C^c\right]^{1/((a+b+c))} + \frac{1}{2} E_g + E_0 \qquad [2]$$

In which a, b, and c are the number of atoms in the compounds. The values of Eg and χ (Mullikens electronegativity of atoms) for MgFe-LDH$_{cal}$ are 1.8 and 5.72 eV, respectively. Therefore, the E_{CB} and E_{VB} of MgFe-LDH$_{cal}$ were calculated to be -0.32 and +1.48 eV versus normal hydrogen electrode (NHE). In addition, Eg and χ values for TiO$_2$ are 3.2 and 5.81 eV, respectively. Furthermore, E_{CB} and E_{VB} for TiO$_2$ were calculated to be -0.29 and +2.91 eV/NHE, respectively. When the MgFe-LDH$_{cal}$/TiO$_2$ heterojunction were irradiated by the visible light, the photons attaining to the photocatalyst would be absorbed by MgFe-LDH$_{cal}$ due to its narrow band gap leading to generation of some electron-hole pairs. As can be seen in Figure 10, the CB of MgFe-LDH$_{cal}$ is higher than that of TiO$_2$. Hence, the photogenerated electrons in the CB of MgFe-LDH$_{cal}$ can be transferred to TiO$_2$ CB. But due to wider band gap of TiO$_2$, visible light cannot excite the VB electrons to the CB as it is active only under UV

light. These interfacial charge transfers prolong lifetime of the charge carrier by suppressing the recombination of electron-hole pairs, which is more favorable to increase the photocatalytic activity. Some of the photogenerated electrons on the CB of MgFe-LDH$_{cal}$ react with adsorbed O_2 to form $^{o}O_2^{-}$ radicals which may be responsible for the degradation of the dyes. And the holes available in the VB of MgFe-LDH$_{cal}$ could directly oxidize the dyes to get the unpolluted water. So finally, we can predict that the CB electron of TiO_2 and the VB holes are responsible for the overall degradation of the organic/reactive/industrial dyes.

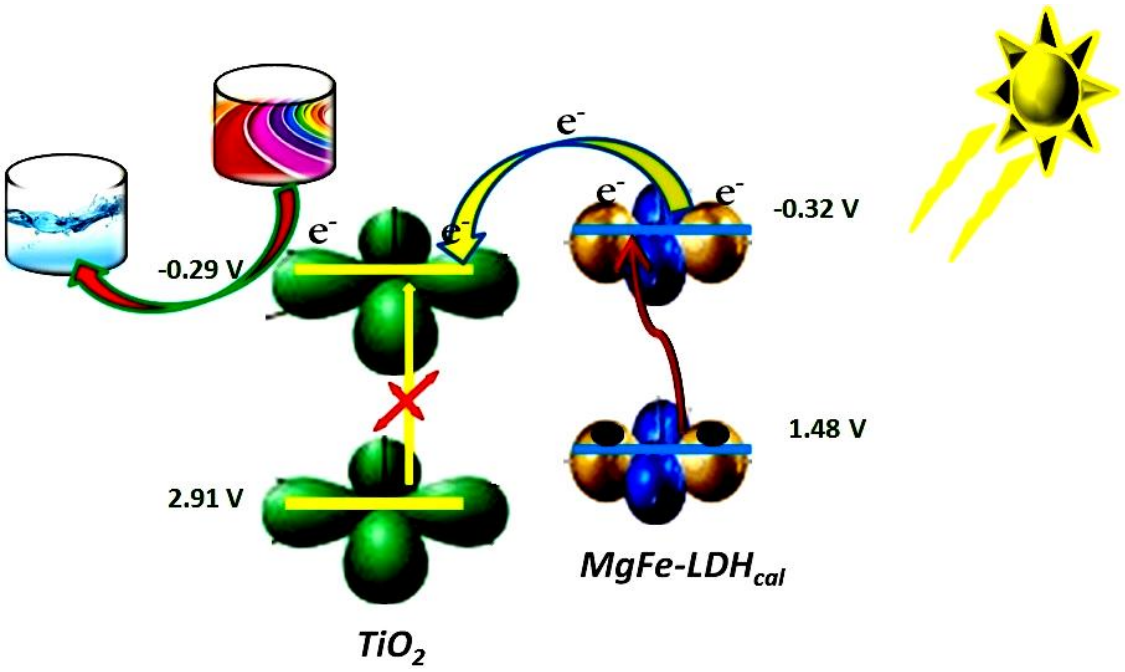

Figure 11. Plausible mechanism for the charge carrier separation in 5MgFe-LDH$_{cal}$/TiO_2 heterojunction.

6. Conclusion

TiO_2-incorporated MgFe-LDHcal nanocomposites were synthesised in this study utilising a cost-effective co-precipitation approach with varied doses to improve textile dye degradation. XRD confirmed the presence of calcined MgFe-LDH and anatase TiO_2 phases without any impurities. The morphology of composites was recorded using TEM, and HR-TEM computed interplanar d-spacing (0.45 and 0.33 nm) that was well matched with XRD. In comparison to doped free samples, TiO_2-incorporated MgFe-LDHcal nanocomposites demonstrated superior catalytic activity of up to 99.9%. This study evaluates a thorough analysis of the photocatalytic degradation of the reactive class dyes *Ca*. By using layered double hydroxide (LDH) and TiO_2 heterojunction (MgFe-LDHcal/TiO_2), the hazardous category dye i.e. reactive green 19, reactive red 120, reactive blue 4, and Eosin Yellowish dye were degraded. For the first time, the photocatalytic use of the aforementioned heterojunction was examined. The most important future development in this area will be the development of a large scale synthesis reactor that can use direct industrial effluents for treat the hazardous materials present in waste water.

Acknowledgements
Alaka Samal is thankful to UGC, India for the grant of Dr. D. S. Kothari Postdoctoral Fellowship. Authors are thankful to Council for Scientific and Industrial Research, NEW DELHI, INDIA for funding of CSIR network project (CSC-135).

Competing Interests
The authors declare no competing interests.

References
1. Kim, S., Park, C., Kim, T. H., Lee, J., & Kim, S. W. (2003). COD reduction and decolorization of textile effluent using a combined process. Journal of Bioscience and Bioengineering, 95(1), 102–105. https://doi.org/10.1016/s1389-1723(03)80156-1.
2. O'Neill, C., Hawkes, F. R., Hawkes, D. L., Lourenço, N. D., Pinheiro, H. M., & Delée, W. (1999, November). Colour in textile effluents - sources, measurement, discharge consents and simulation: a review. Journal of Chemical Technology & Biotechnology, 74(11), 1009–1018. http://dx.doi.org/10.1002/(sici)1097-4660(199911)74:11<1009::aid-jctb153>3.0.co;2-n.
3. GONG, R., LI, M., YANG, C., SUN, Y., & CHEN, J. (2005, May 20). Removal of cationic dyes from aqueous solution by adsorption on peanut hull. Journal of Hazardous Materials, 121(1–3), 247–250. https://doi.org/10.1016/j.jhazmat.2005.01.029.
4. Pharma, R. (2010, January). Zulassungserweiterung für Grippemedikament. MMW - Fortschritte Der Medizin, 152(5), 46–46. https://doi.org/10.1007/bf03366016.
5. Iqbal, M. J., & Ashiq, M. N. (2007, January). Adsorption of dyes from aqueous solutions on activated charcoal. Journal of Hazardous Materials, 139(1), 57–66. https://doi.org/10.1016/j.jhazmat.2006.06.007.
6. Khataee, A., Pons, M., & Zahraa, O. (2009, August 30). Photocatalytic degradation of three azo dyes using immobilized TiO2 nanoparticles on glass plates activated by UV light irradiation: Influence of dye molecular structure. Journal of Hazardous Materials, 168(1), 451–457. https://doi.org/10.1016/j.jhazmat.2009.02.052.
7. Gupta, S. M., & Tripathi, M. (2011, May 19). A review of TiO2 nanoparticles. Chinese Science Bulletin, 56(16), 1639–1657. https://doi.org/10.1007/s11434-011-4476-1.
8. Kirchoff, B. K., & Kunze, H. (1995, March). Inflorescence and Floral Development in Orchidantha maxillarioides (Lowiaceae). International Journal of Plant Sciences, 156(2), 159–171. https://doi.org/10.1086/297237.
9. Huang, C., Dong, C., & Tang, Z. (1993, January). Advanced chemical oxidation: Its present role and potential future in hazardous waste treatment. Waste Management, 13(5–7), 361–377. https://doi.org/10.1016/0956-053x(93)90070-d.
10. Andreozzi, R. (1999, October 15). Advanced oxidation processes (AOP) for water purification and recovery. Catalysis Today, 53(1), 51–59. https://doi.org/10.1016/s0920-5861(99)00102-9.
11. Willmott, N., Guthrie, J., & Nelson, G. (1998, February). The biotechnology approach to colour removal from textile effluent. Journal of the Society of Dyers and Colourists, 114(2), 38–41. https://doi.org/10.1111/j.1478-4408.1998.tb01943.x.
12. Mishra, G., Tripathy, M. 2006. A critical review of the treatments for decolourization of textile effluent.Colourage, 40: 3538.

13. Li, Qin, et al. “Highly Efficient Visible-Light-Driven Photocatalytic Hydrogen Production of CdS-Cluster-Decorated Graphene Nanosheets.” Journal of the American Chemical Society, vol. 133, no. 28, American Chemical Society (ACS), June 2011, pp. 10878–84. Crossref, https://doi.org/10.1021/ja2025454.
14. Liu, Shengwei, et al. “Tunable Photocatalytic Selectivity of Hollow TiO2 Microspheres Composed of Anatase Polyhedra With Exposed {001} Facets.” Journal of the American Chemical Society, vol. 132, no. 34, American Chemical Society (ACS), Aug. 2010, pp. 11914–16. Crossref, https://doi.org/10.1021/ja105283s.
15. Kudo, Takeshi, et al. “Development of Rectangular Column Structured Titanium Oxide Photocatalysts Anchored on Silica Sheets by a Wet Process.” Research on Chemical Intermediates, vol. 29, no. 6, Springer Science and Business Media LLC, Oct. 2003, pp. 631–39. Crossref, https://doi.org/10.1163/156856703322539663.
16. Bahnemann, Detlef. “Photocatalytic Water Treatment: Solar Energy Applications.” Solar Energy, vol. 77, no. 5, Elsevier BV, Nov. 2004, pp. 445–59. Crossref, https://doi.org/10.1016/j.solener.2004.03.031.
17. C. Pulgarin, G.M. Pajonk, J. Bandara, J. Kiwi, Meeting ACS Division of Environmental Chemistry, Anaheim CA Paper No. 232, 1995, p. 767..
18. Zhang, Fenglei, et al. “TiO2-assisted Photodegradation of Dye Pollutants II. Adsorption and Degradation Kinetics of Eosin in TiO2 Dispersions Under Visible Light Irradiation.” Applied Catalysis B: Environmental, vol. 15, no. 1–2, Elsevier BV, Jan. 1998, pp. 147–56. Crossref, https://doi.org/10.1016/s0926-3373(97)00043-x.
19. Liu, Guangming, et al. “Photoassisted Degradation of Dye Pollutants. 8. Irreversible Degradation of Alizarin Red Under Visible Light Radiation in Air-Equilibrated Aqueous TiO2 Dispersions.” Environmental Science & Technology, vol. 33, no. 12, American Chemical Society (ACS), May 1999, pp. 2081–87. Crossref, https://doi.org/10.1021/es9807643.
20. Liu, Guangming, et al. “Photooxidation Mechanism of Dye Alizarin Red in TiO2 Dispersions Under Visible Illumination: An Experimental and Theoretical Examination.” Journal of Molecular Catalysis A: Chemical, vol. 153, no. 1–2, Elsevier BV, Mar. 2000, pp. 221–29. Crossref, https://doi.org/10.1016/s1381-1169(99)00351-9.
21. “Photocatalytic Degradation of Reactive Dyes in Effluents Employing Copper Doped Titanium Dioxide Nanocrystals and Direct Sunlight.” Chemical Science Transactions, vol. 2, no. 4, Chemical Science Transactions, Oct. 2013. Crossref, https://doi.org/10.7598/cst2013.575.
22. Zhu, Jiefang, et al. “Hydrothermal Doping Method for Preparation of Cr3+-TiO2 Photocatalysts With Concentration Gradient Distribution of Cr3+.” Applied Catalysis B: Environmental, vol. 62, no. 3–4, Elsevier BV, Feb. 2006, pp. 329–35. Crossref, https://doi.org/10.1016/j.apcatb.2005.08.013.
23. Zhu, Jiefang, et al. “Characterization of Fe–TiO2 Photocatalysts Synthesized by Hydrothermal Method and Their Photocatalytic Reactivity for Photodegradation of XRG Dye Diluted in Water.” Journal of Molecular Catalysis A: Chemical, vol. 216, no. 1, Elsevier BV, July 2004, pp. 35–43. Crossref, https://doi.org/10.1016/j.molcata.2004.01.008.
24. Di Paola, A., et al. “Preparation of Polycrystalline TiO2 Photocatalysts Impregnated With Various Transition Metal Ions: Characterization and Photocatalytic Activity for the Degradation of 4-Nitrophenol.” The Journal of Physical Chemistry B, vol. 106, no. 3, American Chemical Society (ACS), Dec. 2001, pp. 637–45. Crossref, https://doi.org/10.1021/jp013074l.

25. Ramalingam, G., Perumal, N., Priya, A., & Rajendran, S. (2022, August). A review of graphene-based semiconductors for photocatalytic degradation of pollutants in wastewater. Chemosphere, 300, 134391. https://doi.org/10.1016/j.chemosphere.2022.134391
26. Kim, S., Durand, P., André, E., & Carteret, C. (2017, July). Enhanced photocatalytic ability of Cu, Co doped ZnAl based mixed metal oxides derived from layered double hydroxides. Colloids and Surfaces A: Physicochemical and Engineering Aspects, 524, 43–52. https://doi.org/10.1016/j.colsurfa.2017.04.019
27. Nayak, S., Swain, G., & Parida, K. (2019, May 30). Enhanced Photocatalytic Activities of RhB Degradation and H2 Evolution from in Situ Formation of the Electrostatic Heterostructure MoS2/NiFe LDH Nanocomposite through the Z-Scheme Mechanism via p–n Heterojunctions. ACS Applied Materials & Interfaces, 11(23), 20923–20942. https://doi.org/10.1021/acsami.9b06511
28. Keyikoğlu, R., Doğan, I. N., Khataee, A., Orooji, Y., Kobya, M., & Yoon, Y. (2022, December). Synthesis of visible light responsive ZnCoFe layered double hydroxide towards enhanced photocatalytic activity in water treatment. Chemosphere, 309, 136534. https://doi.org/10.1016/j.chemosphere.2022.136534
29. Parra, Sandra, et al. “Photocatalytic Degradation of Atrazine Using Suspended and Supported TiO2.” Applied Catalysis B: Environmental, vol. 51, no. 2, Elsevier BV, July 2004, pp. 107–16. Crossref, https://doi.org/10.1016/j.apcatb.2004.01.021.
30. Moreira, Regina de Fátima Peralta Muniz, et al. “Mass Transfer and Photocatalytic Degradation of Leather Dye Using TiO2/UV.” Journal of Applied Electrochemistry, vol. 35, no. 7–8, Springer Science and Business Media LLC, July 2005, pp. 821–29. Crossref, https://doi.org/10.1007/s10800-005-5167-x.
31. Samal, Alaka, et al. “3 D Co3(PO4)2-Reduced Graphene Oxide Flowers for Photocatalytic Water Splitting: A Type II Staggered Heterojunction System.” ChemSusChem, vol. 9, no. 22, Wiley, Nov. 2016, pp. 3150–60. Crossref, https://doi.org/10.1002/cssc.201601214.